Shape functions for three-dimensional control-volume mixed finite-element methods on irregular grids

Richard L. Naff [a], Thomas F. Russell [b] * and John D. Wilson [b] †

[a]U.S. Geological Survey, Denver, CO USA

[b]University of Colorado at Denver, Denver, CO USA

Numerical methods based on unstructured grids, with irregular cells, frequently require discrete shape functions to approximate the distribution of quantities across cells. For control-volume mixed finite-element methods, vector shape functions are used to approximate the distribution of velocities across cells. Previous, two-dimensional developments used linear shape functions to interpolate velocities within a quadrilateral cell. For irregular hexahedral cells in three dimensions, it can be shown that linear shape functions cannot exactly represent the flux distribution across a cell under uniform flow conditions. As a result, uniform flow cannot be exactly simulated. A new vector shape function is proposed for use with irregular hexahedral cells that should provide for a more accurate velocity approximation within a cell. This velocity shape function is a non-linear interpolator, containing quadratic terms.

1. INTRODUCTION

For simulation of two-dimensional flow in heterogeneous porous media, it has been shown that mixed methods, and in particular the control-volume mixed finite-element (CVMFE) methods, are often the most accurate methods for solving for the velocity field [1,2]. In this paper, we report on a three-dimensional velocity shape functions, based on covariant vectors for a mapping to a unit cube and for use with irregular hexahedral cells [3]. The three-dimensional algorithm described herein is based on the CVMFE methodology as developed by Cai et al. [2] for the simulation of Darcian flow in two dimensions. In the CVMFE method, the domain is discretized into hexahedral cells that can have irregular shapes, allowing for the modeling of complex hydrogeological systems. Shape functions serve as vector basis functions to interpolate the velocity over the cell interiors. Vector test functions are used as weighting factors for integrating the Darcy relation over control volumes associated with cell faces; this usage can be viewed as an error minimization step in the control volume technique [4]. When used to approximate the Darcy relation, the CVMFE method results in sets of discrete equations from which bulk fluxes at cell faces and pressures at cell centers are solved for. Shape functions have the role of using the estimated bulk fluxes at the cell surface to approximate the

*Supported in part by NSF Grants DMS-9706866 and DMS-0084438 and ARO Grant 37119-GS-AAS.

†Presently at: U.S. Geological Survey, Denver, CO USA

Report Documentation Page

Form Approved
OMB No. 0704-0188

1. REPORT DATE	2. REPORT TYPE	3. DATES COVERED
2006		**00-00-2006 to 00-00-2006**

4. TITLE AND SUBTITLE	5a. CONTRACT NUMBER
Shape Functions for Three-Dimensional Control-Volume Mixed Finite-Element Methods on Irregular Grids	5b. GRANT NUMBER
	5c. PROGRAM ELEMENT NUMBER
6. AUTHOR(S)	5d. PROJECT NUMBER
	5e. TASK NUMBER
	5f. WORK UNIT NUMBER
7. PERFORMING ORGANIZATION NAME(S) AND ADDRESS(ES) **University of Colorado at Denver,Center for Computational Mathematics,PO Box 173364,Denver,CO,80217-3364**	8. PERFORMING ORGANIZATION REPORT NUMBER
9. SPONSORING/MONITORING AGENCY NAME(S) AND ADDRESS(ES)	10. SPONSOR/MONITOR'S ACRONYM(S)
	11. SPONSOR/MONITOR'S REPORT NUMBER(S)

12. DISTRIBUTION/AVAILABILITY STATEMENT
Approved for public release; distribution unlimited

13. SUPPLEMENTARY NOTES

14. ABSTRACT
see report

15. SUBJECT TERMS

16. SECURITY CLASSIFICATION OF:			17. LIMITATION OF ABSTRACT	18. NUMBER OF PAGES	19a. NAME OF RESPONSIBLE PERSON
a. REPORT	b. ABSTRACT	c. THIS PAGE			
unclassified	**unclassified**	**unclassified**		**8**	

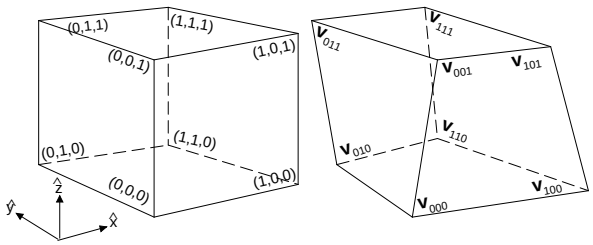

Figure 1. Left: reference cube $\hat{Q}$ with edges of unit length. Right: arbitrary cell Q from discretization with vertex locations $\mathbf{v}_{000}$, $\mathbf{v}_{100}$, $\mathbf{v}_{010}$, $\mathbf{v}_{001}$, $\mathbf{v}_{110}$, $\mathbf{v}_{101}$, $\mathbf{v}_{011}$ and $\mathbf{v}_{111}$ indicated.

velocity in the cell interior. If this approximation is poor, then the solution obtained by the CVMFE method degrades. The velocity shape functions for three-dimensional logically regular meshes proposed in [3] should, in most cases, provide a reasonable cell-velocity estimate. These shape functions are based on a second-order approximation of flux conservation across the cell, which in general provides for a non-linear interpolation of fluxes and the velocities. For three-dimensional flow simulation on irregular meshes, we believe that this function offers advantages over the linear shape function currently used in two-dimensional simulations [2,5].

2. BASIC EQUATIONS

The numerical method outlined in this paper is based on the following steady flow equations applied within a three-dimensional domain Ω:

$$\nabla \cdot \mathbf{q} \;=\; W(x,y,z) \qquad \text{and} \qquad \mathbf{q} \;=\; -\mathbf{K}(x,y,z)\nabla p/\mu, \qquad (x,y,z) \in \Omega. \tag{1}$$

Here $\mathbf{q}$ is the specific discharge vector, $W(x,y,z)$ is a source term, p is the pressure, $\mathbf{K}(x,y,z)$ is the hydraulic conductivity tensor and μ is a general viscosity term. On the surface $\partial\Omega$ of the domain, boundary conditions can consist of specified fluxes over $\partial\Omega_f$ or specified pressures over $\partial\Omega_p$. For the CVMFE method, the hydraulic conductivity tensor is inverted, causing the Darcy relation in (1) to be written as

$$\nabla p \;=\; -\mu\mathbf{K}^{-1}\mathbf{q}. \tag{2}$$

The mixed-method development herein uses the continuity relation from (1) and the inverted Darcy relation from (2) as a basis of the numerical approximation.

The domain Ω is discretized using a logically regular mesh of hexahedral cells, as defined subsequently. This mesh may be irregular in construction to the point where the primary, bounding faces of cells are not planar. Any given hexahedral cell Q can be described from the location of its vertices at $\mathbf{v}_{000}$, $\mathbf{v}_{100}$, $\mathbf{v}_{010}$, $\mathbf{v}_{001}$, $\mathbf{v}_{110}$, $\mathbf{v}_{101}$, $\mathbf{v}_{011}$ and $\mathbf{v}_{111}$, where $\mathbf{v}_{\alpha\beta\gamma} = (x_{\alpha\beta\gamma}, y_{\alpha\beta\gamma}, z_{\alpha\beta\gamma})$ (Figure 1). A trilinear mapping exists such that the hexahedral cell Q is the image of a regular reference hexahedron, $\hat{Q}$, consisting of a unit cube with fixed vertices at $(0,0,0)$, $(1,0,0)$, $(0,1,0)$, $(0,0,1)$, $(1,1,0)$, $(1,0,1)$, $(0,1,1)$ and $(1,1,1)$,

on a point by point basis (see Figure 1). This mapping allows that, for any reference location $\hat{\mathbf{r}} = (\hat{x}, \hat{y}, \hat{z})$ within $\hat{Q}$, the equivalent location $\mathbf{r} = (x, y, z)$ within Q is obtained from the following expression:

$$\mathbf{r} \;=\; \mathbf{v}_o + \mathbf{v}_a\hat{x} + \mathbf{v}_b\hat{y} + \mathbf{v}_c\hat{z} + \mathbf{v}_d\hat{x}\hat{y} + \mathbf{v}_e\hat{x}\hat{z} + \mathbf{v}_f\hat{y}\hat{z} + \mathbf{v}_g\hat{x}\hat{y}\hat{z} \tag{3}$$

where $\mathbf{v}_o = \mathbf{v}_{000}$, $\mathbf{v}_a = \mathbf{v}_{100} - \mathbf{v}_o$, $\mathbf{v}_b = \mathbf{v}_{010} - \mathbf{v}_o$, $\mathbf{v}_c = \mathbf{v}_{001} - \mathbf{v}_o$, $\mathbf{v}_d = \mathbf{v}_{110} - \mathbf{v}_o - \mathbf{v}_a - \mathbf{v}_b$, $\mathbf{v}_e = \mathbf{v}_{101} - \mathbf{v}_o - \mathbf{v}_a - \mathbf{v}_c$, $\mathbf{v}_f = \mathbf{v}_{011} - \mathbf{v}_o - \mathbf{v}_b - \mathbf{v}_c$, $\mathbf{v}_g = \mathbf{v}_{111} - \mathbf{v}_o - \mathbf{v}_a - \mathbf{v}_b - \mathbf{v}_c - \mathbf{v}_d - \mathbf{v}_e - \mathbf{v}_f$. (Also see [2,5].) An irregular mesh of hexahedra Q has a reference mesh of regular cubes; such meshes are referred to as logically regular. Directions associated with the reference mesh are referred to as the logical x, y and z directions. Note that, should $\hat{x}$ be fixed in $\hat{\mathbf{r}}$, then a face normal to the $\hat{x}$ direction within $\hat{Q}$ is determined. This face is mapped, via (3), into an equivalent face within Q. Because $0 \leq \hat{x} \leq 1$, such faces are referred to as intermediate interior cell faces. Covariant vectors, defined as $\mathbf{X}(\hat{y}, \hat{z}) \equiv \partial\mathbf{r}/\partial\hat{x}$, $\mathbf{Y}(\hat{x}, \hat{z}) \equiv \partial\mathbf{r}/\partial\hat{y}$ and $\mathbf{Z}(\hat{x}, \hat{y}) \equiv \partial\mathbf{r}/\partial\hat{z}$, allow for definition of the geometry of Q. The volumetric Jacobian J for passing from Q to $\hat{Q}$ is simply [6]

$$J(\hat{x}, \hat{y}, \hat{z}) \;=\; \mathbf{X}(\hat{y}, \hat{z}) \cdot (\mathbf{Y}(\hat{x}, \hat{z}) \times \mathbf{Z}(\hat{x}, \hat{y})) \tag{4}$$

Surface Jacobians are similarly defined for faces in the logical x, y and z directions [3].

3. VELOCITY SHAPE FUNCTIONS

The shape functions proposed in [3] offer advantages for general hexahedral cells; we present them here. The CVMFE method uses velocity basis vectors, or shape functions, to approximate the Darcy velocity $\mathbf{q}$ in an arbitrary cell Q from bulk fluxes at cell faces. Note that "flux" is defined herein to be the total volumetric discharge through a cell face, as opposed to the volumetric discharge per unit area. The fluxes at every cell face are denoted as f_{x0}, f_{x1}, f_{y0}, f_{y1}, f_{z0} and f_{z1} where, for instance, f_{x0} is the flux through the face at $\hat{x} = 0$. The shape functions for the cell faces are denoted as $\boldsymbol{\nu}_{x0}$, $\boldsymbol{\nu}_{x1}$, $\boldsymbol{\nu}_{y0}$, $\boldsymbol{\nu}_{y1}$, $\boldsymbol{\nu}_{z0}$ and $\boldsymbol{\nu}_{z1}$. Allowing $\mathbf{V}_c$ to be this approximation of $\mathbf{q}$, then its cell-wise representation is

$$\mathbf{V}_c \;=\; f_{x0}\boldsymbol{\nu}_{x0} + f_{x1}\boldsymbol{\nu}_{x1} + f_{y0}\boldsymbol{\nu}_{y0} + f_{y1}\boldsymbol{\nu}_{y1} + f_{z0}\boldsymbol{\nu}_{z0} + f_{z1}\boldsymbol{\nu}_{z1}. \tag{5}$$

The Darcy velocity $\mathbf{q}$ is represented by such a relation for every cell in the mesh. For general hexahedral cells, the shape functions are assumed to have the following form [3]:

$$\boldsymbol{\nu}_{x0} \;=\; \frac{1}{J}[(1-\hat{x})\mathbf{X}\beta_{x0} - \hat{x}(1-\hat{x})\mathbf{X}\beta_{x2}r_{xx0} - \hat{y}(1-\hat{y})\mathbf{Y}\beta_{y2}r_{yx0} - \hat{z}(1-\hat{z})\mathbf{Z}\beta_{z2}r_{zx0}], \tag{6a}$$

$$\boldsymbol{\nu}_{x1} \;=\; \frac{1}{J}[\hat{x}\mathbf{X}\beta_{x1} - \hat{x}(1-\hat{x})\mathbf{X}\beta_{x2}r_{xx1} - \hat{y}(1-\hat{y})\mathbf{Y}\beta_{y2}r_{yx1} - \hat{z}(1-\hat{z})\mathbf{Z}\beta_{z2}r_{zx1}], \tag{6b}$$

$$\boldsymbol{\nu}_{y0} \;=\; \frac{1}{J}[(1-\hat{y})\mathbf{Y}\beta_{y0} - \hat{x}(1-\hat{x})\mathbf{X}\beta_{x2}r_{xy0} - \hat{y}(1-\hat{y})\mathbf{Y}\beta_{y2}r_{yy0} - \hat{z}(1-\hat{z})\mathbf{Z}\beta_{z2}r_{zy0}], \tag{6c}$$

$$\boldsymbol{\nu}_{y1} \;=\; \frac{1}{J}[\hat{y}\mathbf{Y}\beta_{y1} - \hat{x}(1-\hat{x})\mathbf{X}\beta_{x2}r_{xy1} - \hat{y}(1-\hat{y})\mathbf{Y}\beta_{y2}r_{yy1} - \hat{z}(1-\hat{z})\mathbf{Z}\beta_{z2}r_{zy1}], \tag{6d}$$

$$\boldsymbol{\nu}_{z0} \;=\; \frac{1}{J}[(1-\hat{z})\mathbf{Z}\beta_{z0} - \hat{x}(1-\hat{x})\mathbf{X}\beta_{x2}r_{xz0} - \hat{y}(1-\hat{y})\mathbf{Y}\beta_{y2}r_{yz0} - \hat{z}(1-\hat{z})\mathbf{Z}\beta_{z2}r_{zz0}], \tag{6e}$$

$$\boldsymbol{\nu}_{z1} \;=\; \frac{1}{J}[\hat{z}\mathbf{Z}\beta_{z1} - \hat{x}(1-\hat{x})\mathbf{X}\beta_{x2}r_{xz1} - \hat{y}(1-\hat{y})\mathbf{Y}\beta_{y2}r_{yz1} - \hat{z}(1-\hat{z})\mathbf{Z}\beta_{z2}r_{zz1}], \tag{6f}$$

where, for $\kappa = x$, y, or z, and $l = 0, 1$, the r factors in $(6a)$ - $(6f)$ become

$$r_{\kappa xl} = \frac{\mathbf{W}_{2\kappa}}{8} \cdot \sum_{m=0}^{1} \sum_{p=0}^{1} \frac{\beta_{xl}(m,p)\mathbf{X}(m,p)}{J(l,m,p)}, \quad r_{\kappa yl} = \frac{\mathbf{W}_{2\kappa}}{8} \cdot \sum_{m=0}^{1} \sum_{p=0}^{1} \frac{\beta_{yl}(m,p)\mathbf{Y}(m,p)}{J(m,l,p)},$$
$$r_{\kappa zl} = \frac{\mathbf{W}_{2\kappa}}{8} \cdot \sum_{m=0}^{1} \sum_{p=0}^{1} \frac{\beta_{zl}(m,p)\mathbf{Z}(m,p)}{J(m,p,l)}. \tag{7}$$

Here, $J(\hat{x}, \hat{y}, \hat{z})$ is the volumetric Jacobian (4). The factors $\beta_{x\ell}$, $\beta_{y\ell}$ and $\beta_{z\ell}$, for $\ell = 0, 1$ are given by

$$\beta_{x\ell} = |\mathbf{Y} \times \mathbf{Z}| / A_x|_{\hat{x}=\ell}, \quad \beta_{y\ell} = |\mathbf{Z} \times \mathbf{X}| / A_y|_{\hat{y}=\ell}, \quad \beta_{z\ell} = |\mathbf{X} \times \mathbf{Y}| / A_z|_{\hat{z}=\ell}, \tag{8}$$

where $A_x(\hat{x})$, $A_y(\hat{y})$ and $A_z(\hat{z})$ are surface areas of intermediate interior faces:

$$A_x(\hat{x}) = \int_0^1 \int_0^1 |\mathbf{Y} \times \mathbf{Z}|(\hat{x}, \hat{y}, \hat{z})\, d\hat{y}\, d\hat{z}, \quad A_y(\hat{y}) = \int_0^1 \int_0^1 |\mathbf{Z} \times \mathbf{X}|(\hat{x}, \hat{y}, \hat{z})\, d\hat{x}\, d\hat{z},$$
$$A_z(\hat{z}) = \int_0^1 \int_0^1 |\mathbf{X} \times \mathbf{Y}|(\hat{x}, \hat{y}, \hat{z})\, d\hat{x}\, d\hat{y}. \tag{9}$$

Similarly, the expressions for β_{x2}, β_{y2} and β_{z2} are

$$\beta_{x2} = \frac{(\mathbf{Y}_{2x} \times \mathbf{Z}_{2x}) \cdot \mathbf{W}_{2x}}{|\mathbf{W}_{2x}|^2}, \quad \beta_{y2} = \frac{(\mathbf{Z}_{2y} \times \mathbf{X}_{2y}) \cdot \mathbf{W}_{2y}}{|\mathbf{W}_{2y}|^2}, \quad \beta_{z2} = \frac{(\mathbf{X}_{2z} \times \mathbf{Y}_{2z}) \cdot \mathbf{W}_{2z}}{|\mathbf{W}_{2z}|^2}. \tag{10}$$

Just as the cross products in (8) define cell surfaces, the cross products contained in (10) define a set of secondary surfaces. The vectors $\mathbf{W}_{2x}$, $\mathbf{W}_{2y}$ and $\mathbf{W}_{2z}$ take the form

$$\mathbf{W}_{2x} = \mathbf{Y}_{2x}(1/2) \times \mathbf{Z}_{2x}(1/2), \quad \mathbf{W}_{2y} = \mathbf{Z}_{2y}(1/2) \times \mathbf{X}_{2y}(1/2),$$
$$\mathbf{W}_{2z} = \mathbf{X}_{2z}(1/2) \times \mathbf{Y}_{2z}(1/2). \tag{11}$$

The vectors associated with secondary surfaces are: $\mathbf{X}_{2z}(\hat{y}) = \mathbf{X}|_{\hat{z}=1} - \mathbf{X}|_{\hat{z}=0}$, $\mathbf{X}_{2y}(\hat{z}) = \mathbf{X}|_{\hat{y}=1} - \mathbf{X}|_{\hat{y}=0}$, $\mathbf{Y}_{2x}(\hat{z}) = \mathbf{Y}|_{\hat{x}=1} - \mathbf{Y}|_{\hat{x}=0}$, $\mathbf{Y}_{2z}(\hat{x}) = \mathbf{Y}|_{\hat{z}=1} - \mathbf{Y}|_{\hat{z}=0}$, $\mathbf{Z}_{2x}(\hat{y}) = \mathbf{Z}|_{\hat{x}=1} - \mathbf{Z}|_{\hat{x}=0}$ and $\mathbf{Z}_{2y}(\hat{x}) = \mathbf{Z}|_{\hat{y}=1} - \mathbf{Z}|_{\hat{y}=0}$. It is shown in [3] that $(6a)$–$(6f)$ are second-order correct in approximation. Note that if shape functions were approximated with linear forms then only the first term in each of $(6a)$–$(6f)$ would be present [4]. If the mesh elements are parallelepipeds, then the quadratic terms in $(6a)$–$(6f)$ will all be null; for such regular meshes, there is no advantage to these shape functions.

Using (5) to represent $\mathbf{q}$ in (1), the following discrete continuity equation results when both sides of the continuity equation in (1) are integrated over Q:

$$f_{x1} - f_{x0} + f_{y1} - f_{y0} + f_{z1} - f_{z0} = \int_Q W(x, y, z)\, dxdydz. \tag{12}$$

This result follows from Gauss' divergence theorem and properties of shape functions [3]. A set of discrete Darcy relations are obtained by integrating (2) against a test function over subdomains spanning all cell faces of the discretized domain [2–4]; an equation similar to (5) is used to approximate $\mathbf{q}$ in these subdomains. The discrete Darcy relation and the discrete continuity equation (12), applied to every cell within the domain, form the sets of equations which are the basis of the CVMFE method.

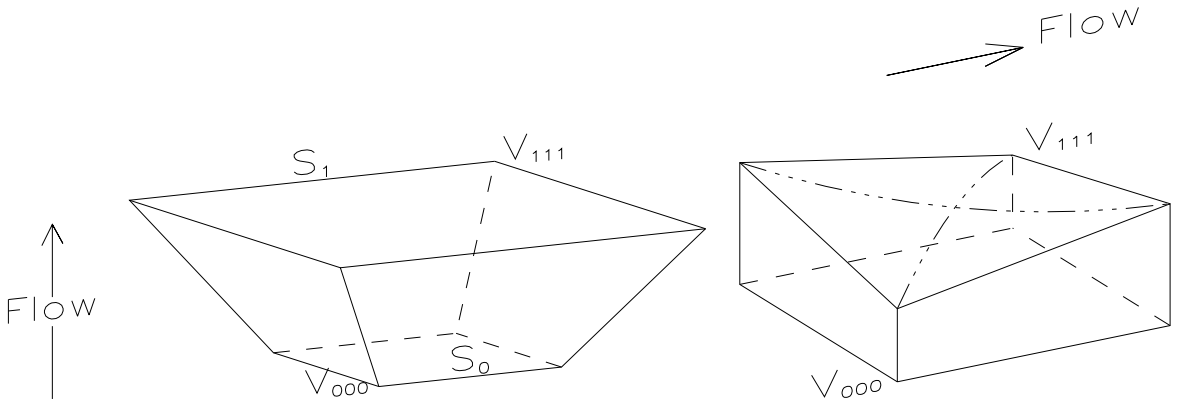

a. Truncated pyramid. b. Tent with curved roof.

Figure 2. a. Hexahedral cell in form of a truncated pyramid. Uniform flow parallel to vertical z axis, as indicated by arrow, is assumed. s_0 and s_1 indicate the length of the lower and upper edges, respectively. b. Hexahedral cell in form of a tent with curved roof. Uniform flow parallel to horizontal x axis, as indicated by arrow, is assumed. Dash-dot lines show maxima and minima of saddle surface forming cell face $\hat{z} = 1$. For both figures, vertices $\mathbf{v}_{000}$ and $\mathbf{v}_{111}$ are indicated; see Figure 1 for orientation.

4. UNIFORM FLOW TESTS

For general hexahedral cells and under uniform flow, linear shape functions of the Piola type will not give the proper flux through an arbitrary cell face. As a simple example, consider the "truncated pyramid" hexahedron Q (Figure 2a), whose bottom face at $z = (s_0 - s_1)/2$ ($\hat{z} = 0$) is a square of side s_0 given by $-s_0/2 \le x \le s_0/2$, $-s_0/2 \le y \le s_0/2$ (with area s_0^2), and whose top face at $z = (s_1 - s_0)/2$ ($\hat{z} = 1$) is the square of side s_1 given by $-s_1/2 \le x \le s_1/2$, $-s_1/2 \le y \le s_1/2$ (with area s_1^2):

$$x \;=\; a(2\hat{x} - 1)/2,\; y \;=\; a(2\hat{y} - 1)/2,\; z \;=\; (\hat{z} - 1/2)(s_1 - s_0) \tag{13}$$

where $a = s_0 + \hat{z}(s_1 - s_0)$. The four lateral faces are planar trapezoids (see Figure 2a). For a unit vertical uniform flow $\mathbf{q} \equiv (0, 0, 1)$, the exact flux across horizontal interior faces for fixed $\hat{z}$ is the cross-sectional area,

$$f_z(\hat{z}) \;=\; [(1 - \hat{z})s_0 + \hat{z}s_1]^2. \tag{14}$$

A linear shape function, while producing the correct fluxes at the top and bottom, will approximate the flux at a face $\hat{z}$ as

$$f_z(\hat{z}) \;\approx\; (1 - \hat{z})f_z(0) + \hat{z}f_z(1) = (1 - \hat{z})s_0^2 + \hat{z}s_1^2. \tag{15}$$

A quadratic flux interpolation, of the type contained in $(6a)$–$(6f)$, can deal exactly with this example. For uniform flow in general, (5) with these shape functions gives an exact cell velocity interpolation if the primary cell faces and secondary surfaces (defined after (10)) are all planar [3]. Mesh construction can usually produce planar primary faces, but

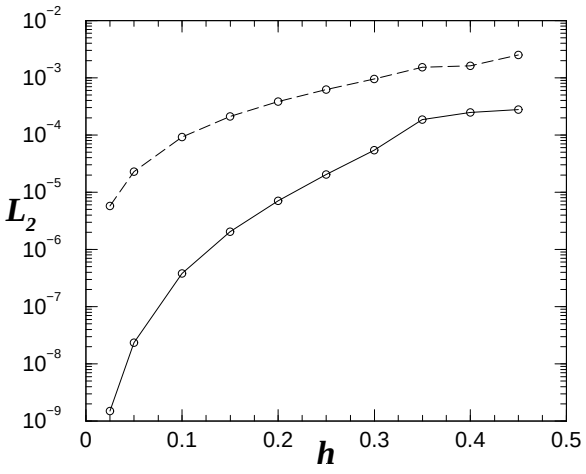

Figure 3. L_2 norm for mesh composed of cells with quasi-random planar faces; see text for h. Solid line: non-linear shape function; Dashed line: linear shape function.

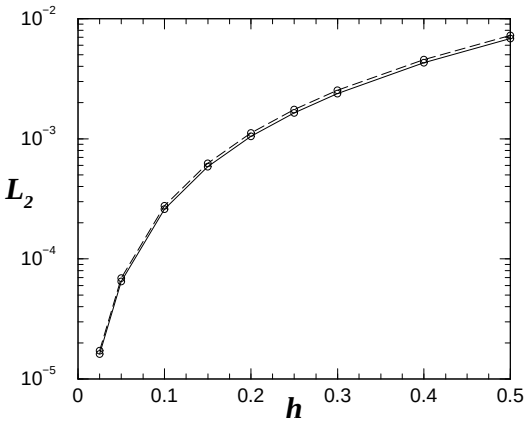

Figure 4. L_2 norm for mesh composed of cells with random vertices; see text for h. Solid line: non-linear shape function; Dashed line: linear shape function.

planar secondary surfaces can be more problematic; in particular, secondary surfaces can be non-planar even when all exterior cell faces are planar. However, our experience has been that, even if the secondary surfaces are non-planar, quite reasonable results can be obtained as long as the primary faces are planar [3]. Planar secondary surfaces can be forced by insisting that each cell have at least one pair of parallel opposite faces.

Use of shape functions $(6a)$–$(6f)$ becomes problematic when the primary faces are non-planar; an example of a non-planar primary face is the "tent with curved roof" (Figure 2b) with unit square base at $z = 0$ ($\hat{z} = 0$), vertical lateral faces, and roof height h_0 at two opposite vertices $(0, 0, h_0)$, $(1, 1, h_0)$ and height h_1 at the other two vertices:

$$x = \hat{x},\ y = \hat{y},\ z = (h_0[(1-\hat{x})(1-\hat{y}) + \hat{x}\hat{y}] + h_1[(1-\hat{x})\hat{y} + \hat{x}(1-\hat{y})])\hat{z}. \tag{16}$$

In $(6a)$–$(6f)$ the covariant vectors $\mathbf{X}$, $\mathbf{Y}$ and $\mathbf{Z}$ provide the directional underpinnings for the shape functions. However, at face $\hat{z} = 1$, $\mathbf{X}$, $\mathbf{Y}$, and $(1-\hat{z})\mathbf{Z}$ all have null normal component, and $f_{z1} = 0$ in (5) for $\mathbf{q} \equiv (1, 0, 0)$. Thus $\mathbf{V}_c$ in (5) has null normal component at all points, while $\mathbf{q}$ does not. Hence $(6a)$–$(6f)$ cannot interpolate uniform $\mathbf{q}$ exactly.

Two sets of simulations were performed to demonstrate these effects; in all cases, meshes with $8 \times 8 \times 8$ cells were used. In the first, irregular cells with planar, quasi-random faces were generated, starting with random vertices on three adjoining exterior faces of Ω. These vertices were created from a regular, two-dimensional mesh on each face by adding to each regular vertex location a uniform random variable from the interval $(-h/2, h/2)$. Starting at the corner where the three exterior faces meet, cells were created by connecting vertices of three existing cell faces to an interior vertex, requiring that the new cell faces forming this connection be planar. This results in interior cells with planar faces, none

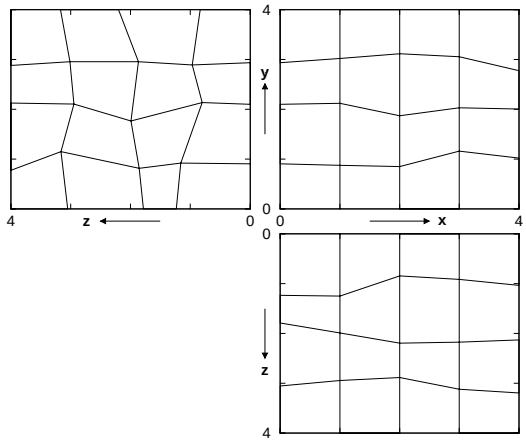

Figure 5. Example of three exterior faces of a 4x4x4 domain that share vertex (0,0,0). Fold up the left (yz) face along the y-axis and the bottom (xz) face along the x-axis. Randomness of vertex locations is exaggerated.

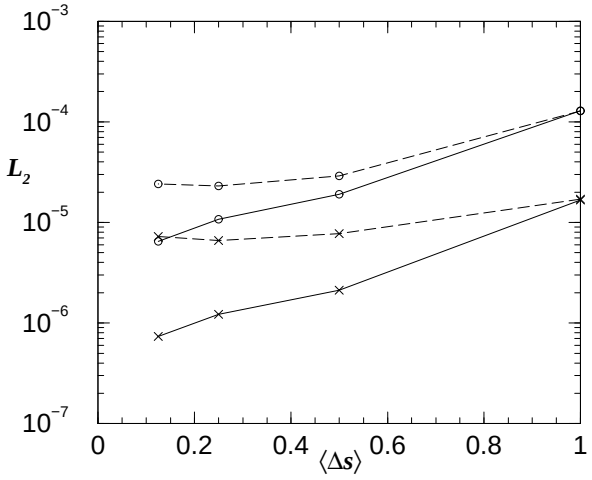

Figure 6. L_2 norm for mesh composed of cells with quasi-random planar faces; see text for $\langle \Delta s \rangle$. Solid line: non-linear shape function; Dashed line: linear shape function; Circle: d is one domain length; Cross: d is two domain lengths.

of which are parallel. The secondary surfaces of cells in this grid are rarely, if ever, planar. Error in simulating uniform flow parallel to the x direction with meshes of this type was quantified using the L_2 norm [4]. Figure 3 is a depiction of the L_2 norm results for this case; increasing h caused successive meshes to be increasingly irregular. These results demonstrate the superiority of the non-linear shape function over the linear shape function for simulating uniform flow. As the secondary surfaces associated with vectors $\mathbf{X}_{2y}$, $\mathbf{X}_{2z}$, $\mathbf{Y}_{2x}$, $\mathbf{Y}_{2z}$, $\mathbf{Z}_{2x}$ and $\mathbf{Z}_{2y}$ are non-planar, the non-linear shape function provides an improved result, but not an exact result. In the second set of simulations (Figure 4), the mesh was created by perturbing all the vertex locations of a regular mesh with a uniform random variable; the vertices on $\partial\Omega$ were perturbed only within the plane forming the surface. This procedure results in meshes where none of the cell faces interior to Ω are planar; uniform flow in the x direction was simulated. The results shown in Figure 4 indicate no particular advantage for the non-linear shape function. As this set of simulations primarily tests the non-planar aspect of the primary cell faces, these results confirm the observations regarding the 'tent with curved roof" cell depicted in Figure 2b.

5. NON-UNIFORM FLOW TESTS

For non-uniform flow, a dipole test was devised whereby a cubic domain (four units on a side) was located midway between a source and a sink of equal strength; the domain was oriented such that the edge $y = 0$, $z = 0$ coincided with a straight line between the poles. The distance from a dipole to the closest domain corner d was allowed to be either one or two domain lengths. Flux boundary conditions for the simulations were

obtained by integrating the normal component of the dipole velocities over the exterior of the domain; these boundary flux estimates were generally very accurate. Quasi-random meshes with planar faces were generated by the same method as before, except that now all cell faces perpendicular to the x direction are parallel (Figure 5); vertices on the exterior faces were randomized in the y and z directions with a uniform random variable from the interval $(-0.1, 0.1)$. This procedure results in planar secondary surfaces for all cells [3]. Meshes with $4\times4\times4$, $8\times8\times8$, $16\times16\times16$ and $32\times32\times32$ cells were generated in this manner, corresponding to mean discretization lengths $\langle\Delta s\rangle$ of 1, 1/2, 1/4 and 1/8 respectively. The results from these simulations, characterized by their L_2 norms, are depicted in Figure 6. These results indicate that, at the coarsest discretization, the error from approximating non-uniform flow overwhelms any corrective effect of the non-linear shape function on the simulation. This error results because the flux estimates on the cell surfaces produced by CVMFE are average or bulk estimates. However, with refinement of the grid (decreasing $\langle\Delta s\rangle$), the non-linear shape function outperforms the linear shape function; with $\langle\Delta s\rangle = 1/8$, an order of magnitude difference can be observed. This results, in large part, because the linear shape functions cease to provide improvement in performance with increased grid refinement when the discretization is quasi-random (see [3] for a more theoretical discussion of the linear/non-linear shape function behavior).

6. CONCLUDING REMARKS

In [3] we note that the convergence of CVMFE, with shape functions $(6a)$–$(6f)$, is second order. Here it is demonstrated that the non-linear shape functions can provide for better resolution of uniform flow with general meshes, relative to linear shape functions, provided that primary cell faces are planar. For non-uniform flow, the level of mesh refinement is all important; only when a general grid is relatively fine will the non-linear aspects of the proposed shape functions contribute significantly.

REFERENCES

1. L. J. Durlofsky. Accuracy of mixed and control volume finite element approximations to Darcy velocity and related quantities. *Water Resour. Res.*, 30(4):965–973, 1994.
2. Z. Cai, J. E. Jones, S. F. McCormick, and T. F. Russell. Control volume mixed finite element methods. *Computational Geosciences*, 1:289–315, 1997.
3. R. L. Naff, T. F. Russell, and J. D. Wilson. Shape functions for velocity interpolation in general hexahedral cells. *Computational Geosciences*, in press, 2002.
4. R. L. Naff, T. F. Russell, and J. D. Wilson. Test functions for three-dimensional control-volume mixed finite-element methods on irregular grids. In L. R. Bentley et al., editors, *Proceedings of the XIII International Conference on Computational Methods in Water Resources, Calgary, Alberta, Canada, 25-29 June, 2000*, pages 677–684. A. A. Balkema, 2000.
5. V. A. Garanzha and V. N. Konshin. Approximation schemes and discrete well models for the numerical simulation of the 2-d non-Darcy fluid flows in porous media. Comm. on appl. math., Computer Centre, Russian Academy of Science, Moscow, 1999.
6. F. B. Hildebrand. *Advanced Calculus for Applications.* Prentice-Hall, Englewood Cliffs, 1962.